Intermediate bands in type-II silicon clathrate with Cu and Ag guest atoms

Zhaohui Huang, Huashan Li, Mark T. Lusk, and Zhigang Wu

Phys. Rev. B **95**, 195208 — Published 15 May 2017

DOI: 10.1103/PhysRevB.95.195208

Intermediate bands in type-II silicon clathrate with Cu and Ag guest atoms

Zhaohui Huang, Huashan Li,* Mark T. Lusk, and Zhigang Wu†
Department of Physics, Colorado School of Mines, Golden, CO 80401, USA‡
(Dated: April 11, 2017)

The unique host-guest structure of the type-II silicon (Si) clathrate offers tunable electronic structures by doping guest atoms or molecules to the Si_{28} cages. Here we investigate the possibility of inducing intermediate bands (IBs) by Cu and Ag atoms employing first-principles calculations based on the density functional theory. Our analyses reveal that one or two isolated Cu/Ag atoms around the cage center are required to obtain IBs useful for photovoltaics; however, further clustering is likely to occur, which removes IBs and converts these Si clathrates into metal. Specifically, the formation of Cu and Ag clusters is mainly determined by local thermodynamics and local kinetics, respectively. All the Cu-clathrate structures presenting IBs are not energetically favorable, making Cu inappropriate for IB solar cells, whereas clathrates with one or two Ag atoms inside the cage that have IBs are thermodynamically stable, but the subsequent aggregation to form 3Ag- or 4Ag-cluster will destroy IBs. Thus preventing clustering is crucial to realize IBs in Si clathates by doping noble metal atoms.

PACS numbers: 71.28.+d, 71.20.-b, 71.15.Mb

I. INTRODUCTION

Silicon (Si) is the most widely used and the best known semiconductor in electronics and optoelectronics. Besides the common diamond bulk phase, Si can also crystalize into highly stable expanded frameworks known as clathrate,[1] whose fundamental building blocks are face-sharing polyhedrons (cages). Because of ample empty space of cages, the interaction between guests (atoms and molecules) and clathrate is normally weak, as suggested by much larger magnitude and stronger temperature dependence of the isotropic atomic displacement parameters of guest atoms than those for Si atoms.[2] The distinctive thermal and vibrational properties of filled clathrate, especially the soft phonon modes from guest atoms,[3] have been intensively studied.[4–6] The weak interaction between guests and host facilitates tuning electronic, optical and dynamical properties of clathrates;[7] as a result, they exhibit many intriguing physical properties, such as glasslike thermal conductivity,[8] superconductivity in sp^3 covalent bonded solids[9,10] and magnetism.[11,12] Recently, Si clathrate materials have attracted intense research interest for applications including lithium ion batteries,[13] thermoelectrics,[14] photovoltaic (PV) cells and optoelectronics,[15–17] etc.

The guest-host structure feature of clathrates could add intermediate bands (IBs) by guest atoms into the forbidden energy gap of clathrate for building highly efficient IB solar cells. Under the isotropic concentrated sunlight illumination (46,050 suns), the single-gap solar cells can achieve maximum PV efficiency about 41% with a band gap (E_g) of 1.1 eV.[18] With the existence of IBs, besides the usual transitions between conduction bands and valence bands, additional absorption due to transitions involving the IBs occur, leading to an optimal efficiency of 63% by splitting a total band gap of 1.95 eV into two sub-gaps of 0.71 eV and 1.24 eV between the IB and the valence band minimum (VBM) and the conduction band maximum (CBM), respectively.[19] The IBs have been experimentally realized in quantum dot layout[20] and by impurity doping.[21] The unoccupied states of InAs quantum dots grown in GaAs matrix are located inside the energy gap of GaAs, while oxygen doped ZnTe:O shows strong emission in the middle of ZnTe gap, which is caused by oxygen defects.[21]

Based on their constituent cages, clathrate frameworks are classified into structural series denoted by Roman numerals, similar to their isomorphic structures of hydrate clathrate discovered about two centuries ago.[22] In this work we focus on the type-II Si clathrate, which can be synthesized routinely[23] and has been investigated for PV applications.[15–17] The Si–Si bonds in type-II clathrates do not deviate much from the ideal sp^3 tetrahedral bonding in diamond Si. The average bond length is 2.34 Å,[24] and bond angle is near 109.47°. The type-II clathrate is especially suitable for possible IB solar cells because its E_g, 1.86 eV, close to the optimal value of 1.95 eV, and its guest concentration can be varied in a wide range.[25–27] In this work we employ first-principle calculations to investigate electronic structures of type-II clathrates with Ag and Cu guest atoms. Since the substitution of Si atoms on framework by Ag/Cu could happen,[28,29] we will also discuss the effect of such substitution. Before presenting the results, we first outline the computational methodology and modeling involved.

II. COMPUTATIONAL METHODS AND MODELING

Our calculations are performed within the framework of the density functional theory (DFT) implemented in the DMol3[30,31] package. The generalized gradient approximation (GGA[32]) was used for the exchange-correlation functional, and all calculations are spin-polarized. Semicore norm-conserving pseuopotentials[33] and the double numerical plus polarization basis sets are

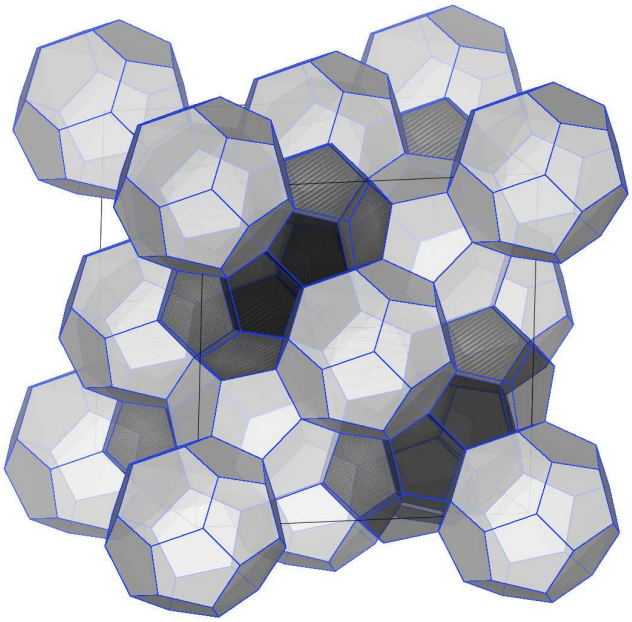

FIG. 1. The conventional unit cell of the type-II clathrate. Si_{28} cages form a cubic diamond network. Four groups of Si_{20} cages, four cages each, occupy the tetrahedral interstices.

employed. A $2\times2\times2$ **k**-grid is used to sample the reciprocal space. Since DFT often severely underestimates band gap, we carry out calculations based on the many-body perturbation theory within the *GW* approximation,[35,36] which is implemented in the Vienna Ab initio Simulation package (VASP).[37–44] The energy cutoff is set at 280 eV, and GW calculations using the plasmon-pole model parameterized by Hybertsen and Louie[35] are performed on a $4 \times 4 \times 4$ **k**-grid. We included 600 conduction bands, and ran ten electronic loops to make sure the two QP energies in the successive loops differ by less than 1 meV. In every electronic loop, the eigenvalues are updated both in G and W, but the eigenstates remain the same as the initial DFT states. The GW band structure is finally interpolated from high-symmetry points. We employ the Nudged Elastic Band[45–47] method implemented in VASP to search kinetic energy barrier, using the projector augmented wave scheme.[48,49] The plane-wave basis set is used up to an energy cutoff of 400 eV. The image chain consists of seven images, and these images are connected by a fictitious spring with a constant at 5 eV/Å^2. The NEB algorithm proceeds until the maximum atomic force is less than 0.02 eV/Å. The final barriers are predicted by spline fitting data.

As shown in Fig. 1, the type-II clathrate consists of two types of cages, eight 28-Si hexakaidecahedra (Si_{28}, point symmetry T_d) and sixteen 20-Si pentagonal dodecahedra (Si_{20}, point symmetry I_h) in a conventional cubic unit cell containing 136 Si atoms. Its structure can be visualized through its dual structure $MgCu_2$,[50] a typical example of the cubic Laves phase. In the type-II clathrate, the symmetric equivalent structure of Mg and Cu atoms are

TABLE I. High symmetry points in the type-II clathate

Wyckoff Positon	Coordinates	Remark
8a	(0.125, 0.125, 0.125)	Tetrahedron center
32e	(0.218, 0.218, 0.218)	Tetrahedron vertices
96g	(0.182, 0.182, 0.371)	Form hexagon
8b	(0.375, 0.375, 0.375)	Si_{28} center
16c	(0.000, 0.000, 0.000)	Si_{20} center

Si_{28} and Si_{20} cages, respectively. In a conventional unit cell, every Si_{28} cage has twelve Si_{20} and four Si_{28} neighboring cages, while every Si_{20} cage is surrounded by six Si_{20} and six Si_{28} neighboring cages. Si_{28} cages form a cubic diamond network, and every four Si_{20} cages occupy a tetrahedral interstice of this diamond network, creating a Si_{20} tetrahedron. The other four tetrahedral interstices are occupied by Si_{28} cages. The relevant Wyckoff positions in the type-II clathrate are listed in Table I.

In this work, we focus on guest atoms in the Si_{28} cages, whereas guest atoms in Si_{20} either have to overcome high kinetic barriers to enter or are not thermodynamically favorable. We model the guest-host system using a conventional unit cell, ensuring guest atoms isolated from each other in different cages. We investigate the diffusion process by searching for the kinetic barrier ($E_{\rm kb}$) that a guest atom has to overcome in order to jump between two neighboring cages and by computing the binding energy ($E_{\rm b}$) defined by

$$E_{\rm b} = (E_{\rm clath} + E_{\rm guest} - E_{\rm total})/N, \qquad (1)$$

where $E_{\rm clath}$, $E_{\rm guest}$ and $E_{\rm total}$ are the total ground-state energies of pure clathrate, guest atoms inside clathrate cages, and the whole structure, respectively. Here E_b indicates the interaction strength between guests and clathrate host. The magnitude of chemical potential (μ), the energy drop to allow an additional guest atom in clathrate, is calculated by

$$\mu = E_{\rm total}(N) - E_{\rm total}(N+1), \qquad (2)$$

where $E_{\rm total}(N)$ represents the total energy of the structure with N guest atoms. μ largely represents the interaction between guest atoms, showing the tendency for a cluster to further grow. The reference cohesive energy are also calculated with DFT technique for comparison.

III. RESULTS

A. Electronic Band Structure of Type-II Clathrate

Fig. 2 plots the DFT and *GW* electronic band structures of the pure type-II clathrate. We find that the *GW* corrections to VBM and CBM are −0.29 and 0.20 eV, respectively, leading to a band gap correction of 0.49 eV,

i.e., increasing the DFT gap of 1.37 eV to the quasiparticle gap of 1.86 eV, in good agreement with previous calculations.[51] Fig. 2 also suggests that the *GW* electronic band structure can be obtained by a scissor shift from the DFT results, and we can estimate the IB position from DFT calculations assuming linear dependence of the energies of the quasiparticle states on the corresponding DFT energies inside the gap. The optimal IB partition, 0.71 eV for the lower sub-gap, roughly corresponds to DFT energy 0.53 eV.

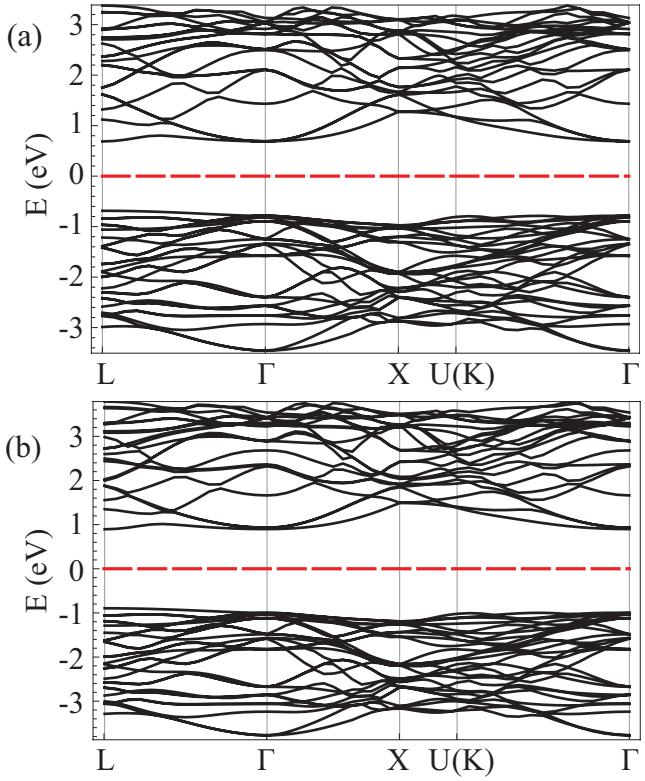

FIG. 2. (a) DFT and (b) *GW* band structures of type-II clathrate. The red dash lines indicate the Fermi level, which is set as energy zero.

B. Cu Guest Atoms in Type-II clathrate

To form IBs in a Si clathrate, the occupied states of guests must be located in the forbidden gap of clathrate and the gust-host interactions shall be weak. We carry out a thorough scan on the elements in the right panel of the periodic table, as well as some diatomic clusters such as GaAs, CuBr, CuS and CdTe. The inert gas atoms could be good candidates since they interact with clathrate very weakly; however, Ar and Kr do not have appropriate energy levels showing up in the clathrate gap. Our investigation suggests that Cu and Ag are most promising among these guests studied.

A Si_{28} cage can contain up to nine Cu atoms, as shown

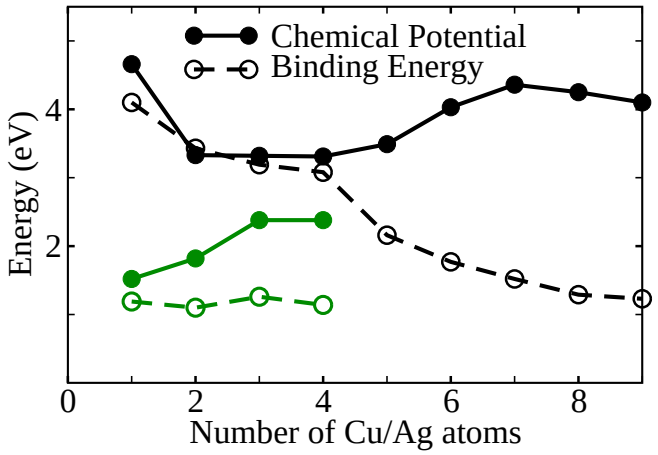

FIG. 3. The highest binding energy (Eq. 1) per guest atom and the maximum of the magnitude of chemical potential (Eq. 2) for adding one more guest atom into a Si_{28} cage are plotted with respect to the number of Cu (black) and Ag (green) guest atoms per conventional unit cell.

in Fig. 3; additional Cu atoms will either break down the Si_{28} cage or be pushed to an adjacent cage. The binding energy between clathrate and Cu-cluster per guest atom decreases with increasing number of Cu, while the magnitude of the chemical potential to form Cu cluster increases once the number of guests is more than four, indicating that Cu atoms tend to aggregate until the geometrical constraints prevent forming clusters larger than 9 Cu atoms. However, when the number of Cu atoms is less than four, the clathrate-Cu binding could counter forming a larger cluster formation, and a Cu-cluster with any size is very difficult to diffuse.

We have computed electronic structures of clathrates with up to 4 Cu atoms per conventional unit cell, whose relaxed configurations (showing only the Si_{28} cage hosting Cu atoms) are summarized in Fig. 4. Their energy comparison for the same number of Cu atoms in a Si_{28} cage is summarized in Table II. The energy reference is taken at the phase of dispersed Cu atoms, where Cu atoms all occupy hexagon centers. Cu atoms always prefer to occupy the center of a Si hexagon, where the Si–Si bonds of the hexagon are expanded to 2.42 Å from 2.34 Å in pure clathrate, and a Cu atom gains charge by 0.69 e, compared to very little charge transfer when it is located around the cage center. Table II also shows that the energy difference between the dispersed phase and the clustered phase continues to decrease with increasing number of Cu atoms until the 4Cu-cluster [Fig. 4(k)] overturns the dispersed phase [Fig. 4(j)] in total energy. Most of the Cu–Cu bonds have a bonding length close to the value (2.55 Å) of the bulk crystal Cu, but it can decrease to 2.47 Å in some cases due to geometrical constraint.

To determine which configurations would exist at thermal equilibrium, in additional to total energy, the kinetic barrier ($E_{\rm kb}$) for Cu guests to diffuse is also crucial. The

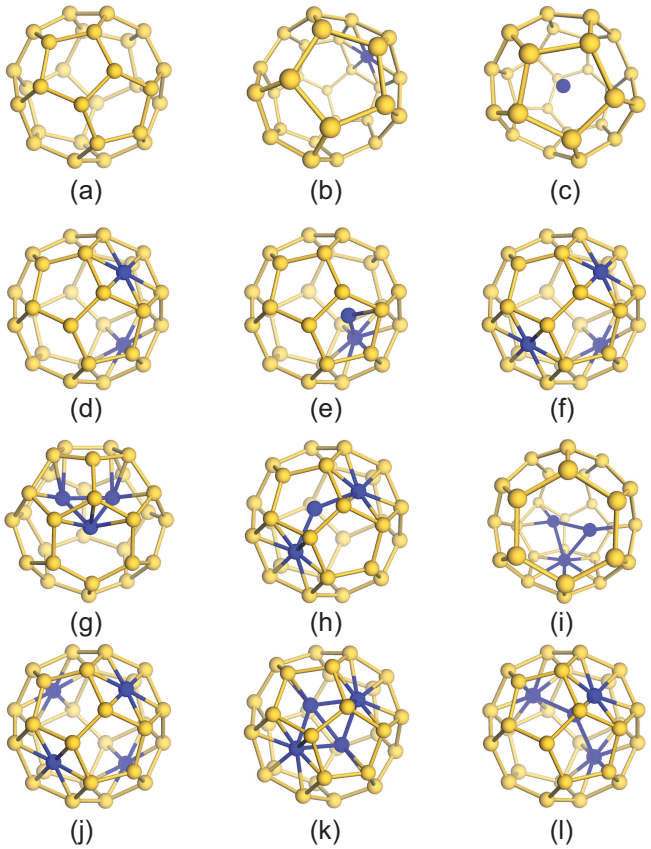

FIG. 4. The relaxed configurations for up to four Cu atoms (deep blue) in a Si_{28} cage (golden) inside one conventional unit cell. (a) Pure clathrate; (b)–(c) one Cu; (d)–(e) two Cu atoms; (f)–(i) three Cu atoms; (j)–(l) Four Cu atoms. The dispersed phase is more stable thermodynamically than the cluster phase until the number of Cu atoms reaches four. See Table II for comparison of total energies.

TABLE II. Relative total energy (ΔE in eV) for a given guest configuration as shown in Fig. 4 for Cu guests and in Fig. 6 for Ag atoms, compared with the configurations with guest atoms dispersed, i.e., those plotted in Figs. 4(b), (d), (f) and (j) as well as Figs. 6(a), (c), (f) and (h).

Cu	ΔE	Ag	ΔE
4(b)	0.0	6(a)	0.0
4(c)	1.54	6(b)	−0.19
Si_{20}[a]	0.92	Si_{20}[a]	−0.28
4(d)	0.0	6(c)	0.0
4(e)	0.33	6(d)	−1.85
4(f)	0.0	6(f)	0.0
4(g)	0.07	6(e)	−2.28
4(h)	0.09		
4(i)	0.21		
4(j)	0.0	6(h)	0.0
4(k)	−0.34	6(g)	−0.47
4(l)	−0.22		
		6(g)6(b)′	0.0[b]
		6(e)6(d)′	−0.11[b]

[a] A single Cu/Ag atom inside the Si_{20} cage.
[b] Ag-cluster of 6(g) or 6(e) in the first cage and one [6(b)] or two [6(d)] Ag atoms in the adjacent cage.

calculated $E_{\rm kb}$ are summarized in Table III. In Fig. 7(a) and Fig. 7(b) we plotted two instances to illustrate the calculation procedure. The barrier is always determined by the path a guest atom takes to pass through a hexagon of Si_{28}. We note that for a Cu guest, a barrier practically represents the energy required for a Cu atom to jump into the cage out of the preferred hexagon center. Although at every step when a Cu atom enters the cage, $E_{\rm kb} > 0$, these barriers are not high enough to prevent Cu atoms from clustering. Thus the most stable configuration is mainly determined by the local thermodynamics.

Fig. 5 summarizes calculated electronic band structures of the type-II clathrates with Cu guests. The corresponding configurations are given in Fig. 4. Presence of Cu guests barely changes the top valence bands of the host, while it lifts the degeneracy of the bottom conduction bands, and we find that more Cu atoms lift the degeneracy more. Our focus here is to search for IBs useful for PV applications, and only in Figs. 5(c), 5(e) the Cu 4*s* states clearly form IBs, and their configurations are given in Figs. 4(c) and 4(e). In both cases there is an Cu atom *inside* the Si_{28} cage, instead of at an hexagon center. However, Table II shows that Figs. 4(c) and 4(e) are not the favored configurations for one and two Cu atoms inside a Si_{28} cage; furthermore, these two configurations can attract more Cu atoms to form larger clusters inside a cage, destroying IBs eventually. Thus we conclude that it is unlikely to use Cu to induce practical IBs in the type-II Si clathrate.

C. Ag Guest Atoms in Type–II Clathrate

Next we discuss Ag atoms as guests in the type-II Si clathrate, in which a Si_{28} cage can hold up to four Ag atoms, and the fifth Ag will be pushed out to the neighboring Si_{28} cage. As shown in Fig. 3, the magnitude of chemical potential for Ag-cluster formation is greater than the corresponding binding energy, i.e., the free energy can be lowered further by clustering than if otherwise Ag guests are dispersed, so Ag atoms will cluster. We also investigate the energetics for all the possible structures with up to four Ag atoms in a Si_{28} cage, as summarized in Fig. 6. In contrast to Cu atoms, which prefer staying at the hexagon centers, Ag atoms interact with the host much weaker with the binding energy about 1.2 eV, compared with $E_{\rm b}$ in the range of 3.1 – 4.1 eV for (up to four) Cu atoms, and they prefer staying inside a Si_{28} cage.

Compared to the cohesive energy per Ag atom in its FCC crystal form, around 2.90 eV by DFT (2.95 eV in

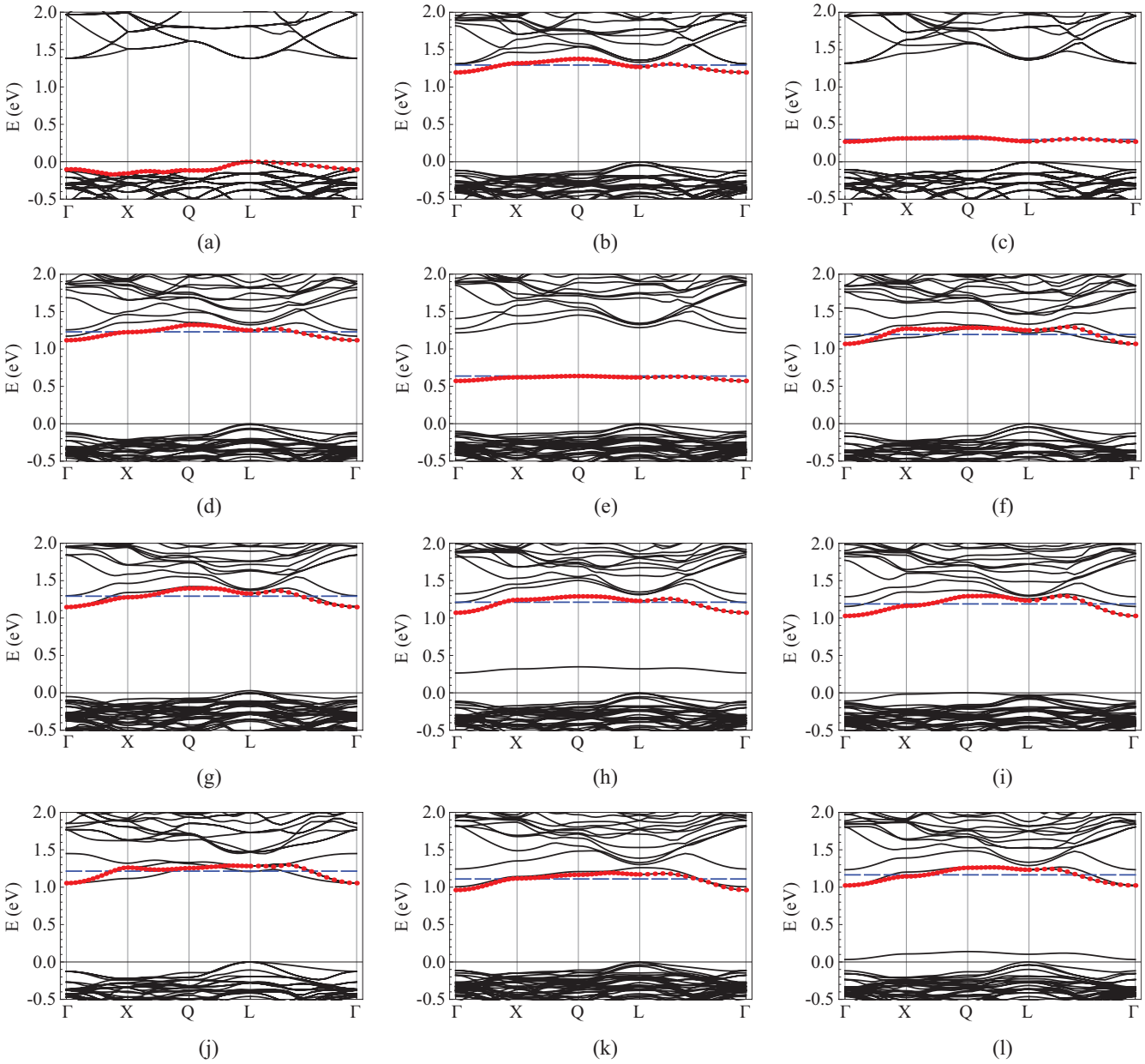

FIG. 5. Electronic band structures of all the configurations given in the same order as in Fig. 4. The Red dotted lines denote the top valence bands of these guest-host systems, while the blue dash lines indicate the Fermi levels. Here the special **k**-points are: Γ (0, 0, 0), X (0, 0, 0.5), Q (0, 0.5, 0.5) and L (0.5, 0.5, 0.5).

experiment[53]), the magnitude of chemical potential for the inclusion of one extra Ag atom in cluster is about 1.80∼2.20 eV. This 0.70∼1.10 eV lowering in free energy will disappear if the substitution of Ag guest for Si in the clathrate occurs, hence the substitution will help cluster formation thermodynamically. In addition, more open space in local structure resulting from substitution also favors diffusion of Ag guest atoms and clustering when a diffused Ag atom encounters another Ag atom or cluster. For the Ag-cluster, the Ag–Ag bond inside a cage ranges from 2.65 to 2.81 Å, shorter than the bulk value of 2.89 Å.[54]

Fig. 8 summarizes calculated electronic band structures of type-II clathrates with Ag guests, whose configurations are plotted in Fig. 6. We find that configurations of Figs. 6(b), 6(d) and 6(h) could provide IBs. Similar to Cu hosts, the Ag atom that is located inside the Si_{28} cage thus weakly interacts with the host provides IBs. However, the configurations plotted in Figs. 6(b) and 6(d) will further cluster when additional Ag atoms are captured, forming structures as plotted in Figs. 6(e) and 6(g), and the IBs will disappear. If an additional Ag atom enters a neighboring cage, a 3Ag-cluster [Fig. 6(h)] would have an IB, as illustrated in Fig. 8(h). But

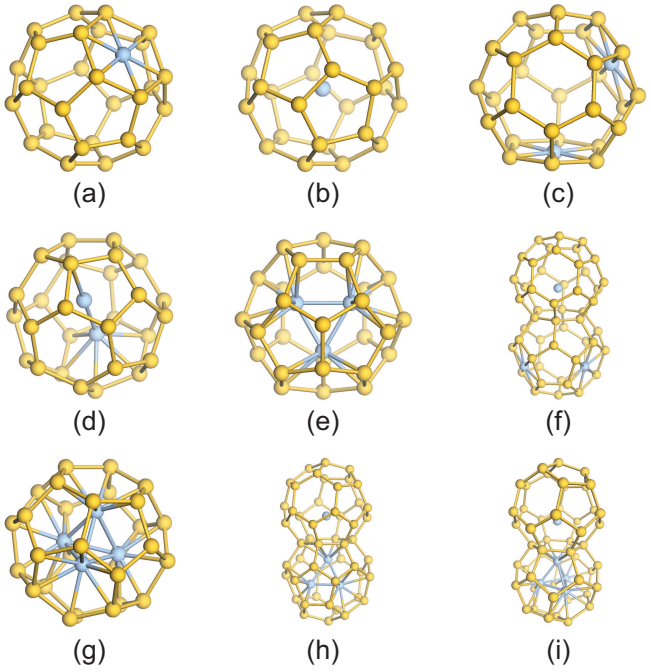

FIG. 6. The relaxed configurations of Ag atoms (light blue) in the Si_{28} cages (golden) in a conventional unit cell. (a)–(b) one Ag atom; (c)–(d) two Ag atoms; (e)–(f) three Ag atoms; and (g)–(h) Four Ag atoms; while (i) shows a satellite Ag atom in a neighboring cage of a 4Ag-cluster.

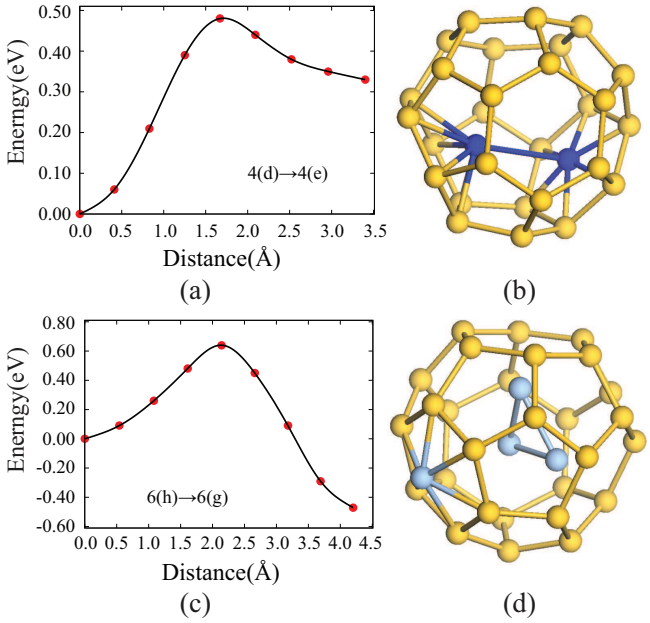

FIG. 7. The kinetic barriers are extracted by spline fitting from seven-image NEB calculations. (a)–(b) corresponds the barrier for 4(d)→4(e). Both Cu atoms intend to jump out of hexagon center. (c)–(d) the barrier on how a 4Ag-cluster begins to form. The barrier prevents the Ag atom in the adjacent cage to pass through the hexagon, but once it enters the cage, it will rush to form the cluster with straight lowering potential energy path.

a 4Ag-cluster with an additional Ag satellite, as plotted in Fig. 6(i), doesn't have a useful IB because the top occupied Ag band is mixed with the bottom conduction bands of clathrate.

We find that the existence of useful IBs of Ag guests depends sensitively on cluster formation in the host, and next we discuss the associated kinetics. As summarized in Table III, an Ag atom has to overcome an energy barrier of 1.63 eV to enter a Si_{28} cage from a Si_{20} cage; therefore, we can assume that Ag atoms diffuse into Si_{28} cages only through the Si_{28}-cage channel. When Ag atoms enter a Si_{28} to cluster, however, the first three Ag atoms do not experience any activation barriers when crossing the Si hexagon centers. Then the fourth Ag atom has to overcome a 0.66 eV kinetic barrier to enter the cage, due largely to the geometric confinement of the Si_{28}. This barrier could make formation of a 4-Ag cluster [Fig. 6(g)] inside a Si_{28} cage more difficult, though it is not high enough to block this process at room temperature.

We also investigate the cluster formation in two Si_{28} cages neighboring to each other. For example, the configuration with two Ag atoms in one cage [Fig. 6(d)] and three in a neighboring one [Fig. 6(e)], has a total energy lower that of the configuration with four Ag atoms in one cage [Fig. 6(g)] and one Ag atom in a neighboring one [Fig. 6(b)]. Thus a 4-Ag cluster is not energetically favored. Furthermore, the kinetics of the same diffusion process also varies with different environment, for example, in contrast to no barrier for the first 3Ag-cluster formation, there is a 0.45 eV barrier for a second 3Ag-cluster to be formed in the neighboring cage; while the presence of a 3Ag-cluster increases the energy barrier for forming a 4Ag-cluster in the neighboring cage from 0.66 eV to 0.79 eV. Given the fact that the largest binding energy per Ag atom barely changes with varying local environment, the Ag-cluster formation is largely determined by its local kinetics.

TABLE III. The kinetic barrier (E_{kb} in eV) for a Cu/Ag guest atom to cross a hexagon of Si clathrate.

Cu	E_{kb}	Ag	E_{kb}
		$Si_{20} \rightarrow 6(b)$[a]	1.63
4(d) → 4(e)	0.48	6(a) → 6(b)	0.08
4(f) → 4(h)	0.32	6(c) → 6(d)	0.0
4(j) → 4(l)	0.29	6(f) → 6(e)	0.0
		6(h) →6(g)	0.66
		6(a)′ → 6(b)′	0.11[b]
		6(f)′ → 6(e)′	0.45[b]
		6(h)′ → 6(g)′	0.79[b]

[a] The barrier for a Ag to enter a Si_{28} cage from a Si_{20} cage.
[b] The barrier for forming a Ag cluster in the second cage with the presence of a 3Ag-cluster in the first cage.

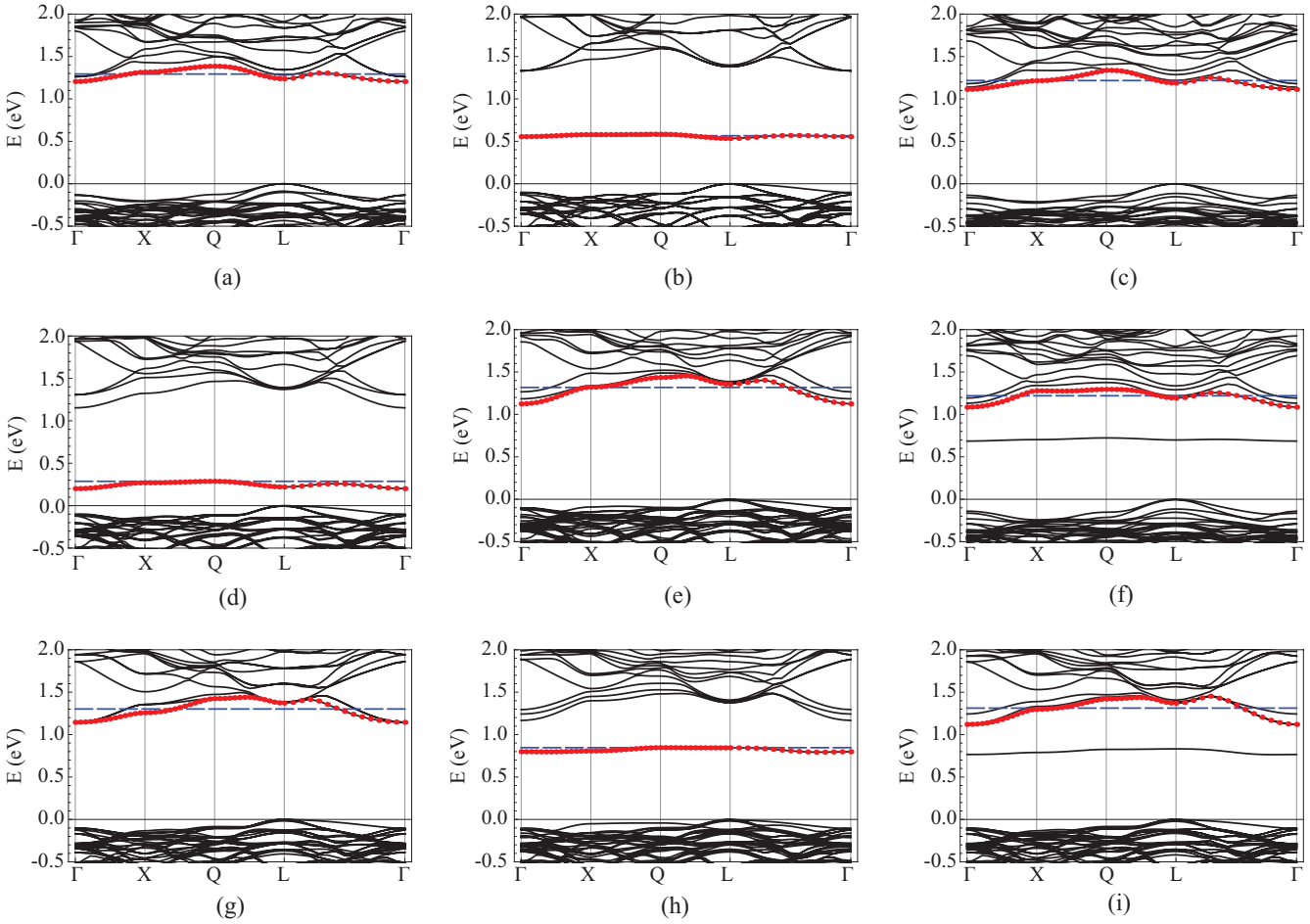

FIG. 8. Electronic band structures of all the configurations listed in the same order as in Fig. 6. The Red dotted lines denote the top valence bands of these guest-host systems, while the blue dash lines indicate the Fermi levels.

D. Electronic Band Structures from the Hybrid Funtional

We also employed the HSE[55] hybrid functional to better describe the localized electronic states of these metallic guest atoms. As shown in Fig. 9, the HSE electronic band structures for configurations of Fig. 4(e) for the Cu guests and Fig. 6(b) for the Ag guests, qualitatively agree with the corresponding GGA band structures plotted in Fig. 5(e) and Fig. 8(b), respectively. Quantitatively, HSE increases E_g in configuration of Fig. 4(e) from GGA value of 1.21 eV to 1.80 eV, in Fig. 6(b) from 1.32 eV to 1.75 eV, in good comparison with the GW band gap of 1.86 eV for the pure type-II Si clathrate. In addition, the relative partitioning of subgaps in both cases barely changes comparing GGA with HSE. Thus we conclude that GGA-DFT band structures for these doped clathrates are qualitatively correct.

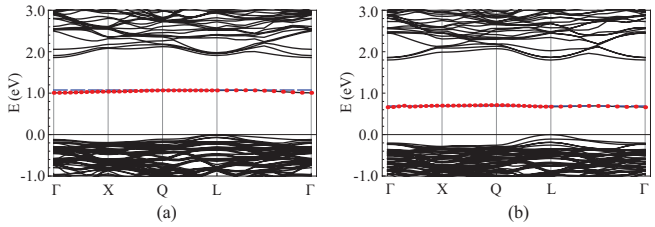

FIG. 9. Electronic band structures for (a) configuration plotted in Fig. 4e and (b) configuration plotted in Fig. 6b, using the HSE hybrid functional. Here the red dotted lines denote the top valence bands of these guest-host systems, while the blue dash lines indicate the Fermi levels.

IV. SUMMARY

Due to its guest-host structure, the electronic band structure of the type-II silicon clathrate can be modified by a range of various guests. Unlike heavy doping in bulk semiconductor causing lattice mismatch and creating strains that accumulate with increasing the number of impurities, ample empty space in cages leads to much

smaller structural distortion for the same doping level; thus it is possible to achieve density of guests a a few orders higher than doping. Optoelectronic devices, especially PV cells, could take advantages of this. Here our first-principles investigation suggests that both Cu and Ag guests in the type- II Si clathrate can lead to IBs for building possible highly efficient solar cells, if they can stay "isolated" inside the Si_{28} cages. But unfortunately, the Cu/Ag guest atoms will inevitably interact with each other and form clusters inside cages, which would make the guest-host system metallic.

Thus the dynamics of clustering is crucial, and our calculations reveal that a Si_{28} cage can hold up to nine Cu atoms. When there are less than four Cu atoms inside a cage, the dispersed phase dominates, and Cu atoms are most likely to be stuck at the hexagon centers; but additional Cu atoms will make the cluster phase thermodynamically favorable. Although there are always low kinetic barriers towards Cu clustering, the large free energy difference mostly decides the stable configurations. On the other hand, the growth of Ag cluster is mainly decided by its kinetics. Ag atoms do not experience sizable kinetic barriers before they form 3Ag-clusters inside the cage, because the Ag atom at the hexagon center deforms the hexagon dramatically and gains substantial charge from clathrate. Once a stable 3Ag-Cluster is formed, an additional Ag atom has to overcome a 0.66 eV kinetic barrier to form a 4Ag-cluster. Moreover, any Ag-cluster presence affects the kinetics in its adjacent cages, indicating that the kinetics could refrain Ag-cluster from growing larger, though the barriers are not high enough to completely stop cluster formation.

We conclude that IBs in type-II clathrate can be induced by one or two Cu/Ag atoms isolated inside the Si_{28} cage, while Cu/Ag clustering will destroy IBs. All Cu-guest configurations with IBs existing are not thermodynamically favorable, whereas the configurations for one or two Ag atoms inside the Si_{28} cage can induce IBs and are thermodynamically stable. But further clustering (3Ag- and 4Ag-clusters) removes IBs, while the saturated cage with 3Ag- or 4Ag-cluster makes it possible for additional Ag atoms in the adjacent cages to create IBs.

Previous experiments[28,29] have shown that Cu or Ag atoms could substitute Si on the clathrate framework. The direct consequence is further weakening of the Si-Cu/Ag bonding and the expanding of local structure, leading to lower kinetic barrier of Cu/Ag atoms diffusion. Therefore, guest atoms clustering is expected to become easier and more severe when substitution occurs. We are investigating all the dynamics involved and the effective approaches to prevent clustering, including the non-equilibrium synthesis such as fast quenching to build spatial lattices and lock all dispersed guest atoms simultaneously.

V. ACKNOWLEDGEMENTS

This work was supported by Renewable Energy Materials Research Science and Engineering Center (REMRSEC), U.S. DOE Early Career Award (Grant No. DE-SC0006433). Computations were carried out at the Golden Energy Computing Organization at CSM and the National Energy Research Scientific Computing Center (NERSC). ZW thanks D. Wood, C. Koh and E. Toberer for insightful discussions.

* Current Address: Department of Materials Science and Engineering, Massachusetts Institute of Technology, Cambridge, MA 02139
† zhiwu@mines.edu
‡ Current Address: Department of Physics, Pennsylvania State University, University Park, PA 16802

[1] A. J. Karttunen, T. F. Fassler, M. Linnnolahti and T. A. Pakkanen, Inorg. Chem. **50**, 1733 (2011).
[2] G. S. Nolas, D. G. Vanderveer, A. P. Wilkinson and J. L. Cohn, J. Appl. Phys. **91**, 8970 (2002).
[3] G. S. Nolas, C. A. Kendziora, J. Gryko, J. J. Dong, C. W. Myles, A. Poddar and O. F. Sankey, J. Appl. Phys. **92**, 7225 (2002).
[4] J. J. Dong, O. F. Sankey and C. W. Myles, Phys. Rev. Lett. **86**, 2361 (2001).
[5] G. S. Nolas, M. Beekman, J. Gryko, G. A. Lamberton Jr., T. M. Tritt and P. F. McMillan, Appl. Phys. Lett. **82**, 910 (2003).
[6] M. A. Avila, K. Suekuni, K. Umeo, H. Fukuoka, S. Yamanka and T. Takabatake, Phys. Rev. B **74**, 125109 (2006).
[7] G. S. Nolas (Editor), "The Physics and Chemistry of Inorganic Clathrates", Springer 2014.
[8] J. L. Cohn, G. S. Nolas, V. Fessatidis, T. H. Metcalf and G. S. Slack, Phys. Rev. Lett. **82**, 779 (1999).
[9] H. Kawaji, H.-O. Horie, S. Yamanaka and M. Ishikawa, Phys. Rev. Lett. **74**, 1427 (1995).
[10] S. Yamanaka, E. Enishi, H. Fukuoka and M. Yasukawa, Inorg. Chem. **39**, 56 (2000).
[11] S. Paschen, W. Carrillo-Cabrera, A. Bentien, V. H. Tran, M. Baenitz, Yu. Grin and F. Steglich, Phys. Rev. B **64**, 214404 (2001).
[12] G. T. Woods, J. Martin, M. Beekman, R. P. Hermann, F. Grandjean, V. Keppens, O. Leupold, G. J. Long and G. S. Nolas, Phys. Rev. B **73**, 174403 (2006).
[13] J. Yang and J. S. Tse, J. Mater. Chem. A **1**, 7782 (2013).
[14] P. Norouzzadeh, C. W. Myles and D. Vashaee, Sci. Rep. **4**, 7028 (2014).
[15] L. L. Baranowski, L. Krishna, A. D. Martinez, T. Rahajo, V. Stevanovic, A. C. Tamboli and E. S. Toberer, J. Mater. chem. C **2**, 3231 (2014).
[16] A. D. Martinez, L. Krishna, L. L. Baranowski, M. T. Lusk, E. S. Toberer. and A C. Tamboli, IEEE J. Photovol. **4**, 1305 (2013).
[17] L. Krishna, A. D. Martinez, L. L. Baranowski, N. P. Brawand, C. A. Koh, V. Stevanovic,, M. T. Lusk, E. S. Toberer. and A C. Tamboli, Proc. IEEE SPIE **8981**, 898108

(2014).
[18] W. Shockley and H. J. Queisser, J. Appl. Phys. **32**, 510 (1961).
[19] A. Luque and A. Marti, Phys. Rev. Lett. **78**, 5014 (1997).
[20] A. Luque, A. Marti and C. Stanley, Nat. Photonics **6**, 146 (2012).
[21] W. Wang, A. S. Lin and J. D. Phillips, Appl. Phys. Lett. **95**, 011103 (2009).
[22] E. D. Sloan, *Clathrate Hydrates of Natural Gases*, Marcel Dekker Inc. New York, 2Ed. (1997).
[23] M. Beekman and G. S. Nolas, J. Mater. Chem. **18**, 842 (2008).
[24] J. Gryko, P. F. Mcmillan, R. F. Marzke, G. K. Ramachandran, D. Patton, S. K. Deb and O. F. Sankey, Phys. Rev. B **62**, R7707 (2000).
[25] M. Beekman and G.S. Nolas, J. Mater. Chem. **18**, 842 (2008).
[26] G.K. Ramachandran, J.J. Dong, J. Diefenbacher, J. Gryko, R.F. Marzke, O.F. Sankey and P.F. McMillan, J. Solid State Chem. **145**, 716 (1999)
[27] E. Reny, P. Gravereau, C. Cros and M. Pouchard, J. Mater. Chem. **8**, 2839 (1998).
[28] G. Cordier and P. Woll, J. Less-Common Metals **169**, 291 (1991).
[29] N. Tsujii, J.H. Roudebush, A. Zevalkink, C.A. Cox-Uvarov, G.J. Snyder and S.M. Kauzlarich, J. Solid State Chem. **184**, 1293 (2011).
[30] B. Delley, J. Chem. Phys. **92**, 508 (1990).
[31] B. Delley, J. chem. Phys. **113**, 7756 (2000).
[32] J. P. Perdew, K. Burke and M. Ernzerhof, Phys. Rev. Lett. **77**, 3865 (1996).
[33] D. R. Hamann, M. Schluter and C. Chiang, Phys. Rev. Lett. **43**, 1494 (1979).
[34] H. J. Monkhorst and J. D. Pack, Phys. Rev. B **13**, 5188 (1976).
[35] M. S. Hybertsen and S. G. Louie, Phys. Rev. B **34**, 5390 (1986).
[36] G. Onida, L. Reining and A. Rubio, Rev. Mod. Phys. **74**, 601 (2002).
[37] G. Kresse and J. Hafner, Phys. Rev. B **47**, 558 (1993).
[38] G. Kresse and J. Hafner, Phys. Rev. B **49**, 14251 (1994).
[39] G. Kresse and J. Furthmüller, Comput. Mat. Sci. **6**, 15 (1996).
[40] G. Kresse and J. Furthmüller, Phys. Rev. B **54**, 11169 (1996).
[41] M. Shishkin and G. Kresse, Phys. Rev. B **74**, 035101 (2006).
[42] M. Shishkin and G. Kresse, Phys. Rev. B **75**, 235102 (2007).
[43] F. Fuchs, J. Furthmüller, F. Bechstedt, M. Shishkin, and G. Kresse, Phys. Rev. B **76**, 115109-1-8 (2007).
[44] M. Shishkin, M. Marsman, and G. Kresse, Phys. Rev. Lett. **99**, 246403 (2007).
[45] H. Jonsson, G. Mills and K. W. Jacobsen, in *Nudged Elastic Band Method for Finding Minimum Energy Paths of Transitions*, in *Classical and Quantum Dynamics in Condensed Phase Simulations, Chap.16*, ed. B. J. Berne, G. Ciccotti and D. F. Coker, World Scientific, 1998.
[46] G. Henkelman, B. P. Uberuaga, and H. Jonsson, J. Chem. Phys. **113**, 9901 (2000).
[47] G. Henkelman and H. Jonsson, J. Chem. Phys. **113**, 9978 (2000).
[48] P. E. Blöchl, Phys. Rev. B **50**, 17953 (1994).
[49] G. Kresse and D. Joubert, Phys. Rev. B, **59**, 1758 (1999).
[50] R. E. Smallman and R. J. Bishop p78, *Modern Physical Metallurgy & Materials Engineering*, butterworth-Heinemann Sixth Edition, 1999.
[51] X. Blase, Phys. Rev. B **67**, 035211 (2003).
[52] M. E. Straumanis and L. S. Yu, Acta Crystallogr. **25A**, 676 (1969).
[53] C. Kittel in "Introduction to Solid State Physics" p50, Hoboken, NJ : John Wiley & Sons Inc., 2005.
[54] L.-G. Liu and W. A. Bassett, J. Appl. Phys. **44**, 1475 (1973).
[55] J. Heyd, G. E. Scuseria, and M. Ernzerhof, J. Chem. Phys. **124**, 219906 (2006).